Structure of Nanometric Silica Clusters in Polymeric Composite Materials

Jacques Persello,[†] Jean-Philippe Boisvert,*[,‡] Aurélien Guyard,[‡] and Bernard Cabane[§]

LCMI, Université de Franche-Comté, 16 route de Gray, 25000 Besançon, France, CRPP, Université du Québec à Trois-Rivières, C.P. 500, Trois-Rivières, Québec, G9A5H7, and PMMH, ESPCI, 10 rue Vauquelin, 75231 Paris, France

Received: November 14, 2003

Composite films were prepared from nanometric silica suspension and poly(vinyl alcohol) (PVA) solution. Both were mixed at increasing silica contents and left until complete evaporation of the solvent. Small angle neutron scattering (SANS) and transmission electron microscopy (TEM) were used to characterize the local and mean particle distribution of silica particles in the film. The interaction between the polymer and the surface was characterized through an adsorption isotherm. The SANS results were processed within the Percus−Yevick approximation. At a given drying stage, the colloidal system undergoes a microphase separation and submicron size clusters are produced. Both SANS and TEM showed the presence of dense and well-ordered clusters in the dry film. The size of the clusters and the surface-to-surface distance between the silica primary particles within the clusters both depend on the initial ionic strength.

Introduction

The use of neutral polymers to improve the colloidal stability of nanosize particles is now well understood and described in numerous textbooks.[1−3] It is known that polymers perform at best in preventing flocculation when they saturate the surface and when their molecular weight (MW) is large enough to allow many trains and loops to protrude toward the bulk solution.[4] In this situation, the osmotic pressure generated by interpenetrating polymer segments between two approaching particles will lead to a repulsive interaction and keep them apart. This behavior is defined as steric repulsion. On the other hand, unsaturated surfaces in the presence of large polymer will promote bridging and the particles will flocculate.[5−8] When the polymer/surface interaction is weak but the surfaces still saturated, the large polymers can lead to the formation of necklaces with many nanoparticles attached to each polymer molecule.[9] The maximum number of particles per necklace depends, among other things, on the electrostatic repulsion between vicinal particles, and consequently, the saturation coverage depends on the ionic strength.

Although the silica/silica interaction in the presence of polymer is well described in dilute conditions with many polymers,[10−12] the behavior of these systems during evaporation is much less understood.[13] This concern is of importance since a whole class of polymeric composite material (i.e. coatings) is often prepared by solvent evaporation. It is well-known that the reinforcing capacity of filler in composites depends on the volume fraction of the filler in the polymer matrix. As an example, according to the Guth and Gold equation,[14] the relative elastic modulus (E/E_0) is a direct function of the volume fraction (ϕ) through the following: $E/E_0 = 1 + 2.5\phi + 14.1\phi^2$. This relationship assumes perfectly dispersed particles within the matrix. The filler particles maximize the possible attachment points with the polymer, i.e. the apparent cross-link density of the matrix, and then maximize the stress at break.[15] These important parameters (modulus and stress at break) depend highly on the distribution of filler particles in the polymer matrix, which in turn depends on the particle/particle interaction (agglomeration) and polymer/particle interactions (adhesion and wetting). Other effects, such as the morphology of the filler particles, have been shown to be of crucial importance. For instance, mica flakes in poly(dimethylsiloxane) lead to composite material with very high modulus and strength as long as they remain dispersed.[15]

Of course, dispersed particles in dilute mixtures will not necessarily remain dispersed as the evaporation progresses. It is known that dispersed particles can rearrange upon concentrating (drying) and lead to evaporation-induced and ordered self-assembly processes.[16] These processes can lead to perfectly ordered liquidlike domains embedded in polymeric matrix, midway between open aggregates and liquidlike fluid. Such behavior has been observed with silica particles in the presence of hydrogen bond reacting polymer[17] but also with grafted polymer.[18] Although much work has been done recently on the understanding of the formation of open silica aggregates in nanocomposites,[19−21] fewer studies have investigated the structural rearrangement occurring in the liquidlike domains when the filler content increases. The control of the self-assembly of nanoparticles into more or less dense but well-ordered clusters presents obvious technological interests and challenges. Conversely, as debated above the homogeneous distribution of nanoparticles is also of importance in the preparation of high-performance nanocomposites.

The main goal of the present work is to investigate the relationship between the polymer/particle interaction in dilute condition and the distribution of particles within the polymer film once solidified. The particles used in this work are monodisperse, spherical, and nanometric silica model particles (hard-sphere radius 13.5 nm), and the polymer is the poly(vinyl alcohol) (PVA) having a gyration radius of 15 nm in the dilute regime. As the evaporation process of the dilute PVA/SiO_2 suspension goes on, the volume fraction, the ionic strength, and the polymer concentration increase. To minimize the number

* Author to whom correspondence should be addressed. Phone: +(819) 376-5075. Fax: +(819) 376-5148. E-mail: jean-philippe_boisvert@uqtr.ca.
[†] LCMI, Université de Franche-Comté.
[‡] CRPP, Université du Québec à Trois-Rivières.
[§] Physico-Chimie Macromoléculaire.

10.1021/jp031249g CCC: $27.50 © 2004 American Chemical Society
Published on Web 06/12/2004

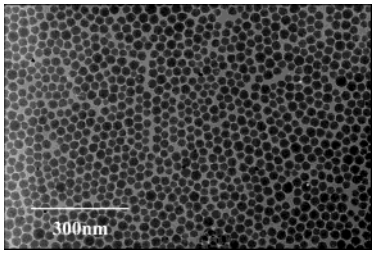

Figure 1. TEM micrograph of the starting silica particles used in the study. The hard-sphere mean particle diameter is 27 nm.

of dependent variables involved, the chosen polymer concentration was high enough to ensure complete saturation with respect to surface coverage. The polymer/surface interaction was adjusted to have a low PVA surface coverage and the ionic strength was not high enough to promote aggregation in the starting conditions.

The use of silica model nanoparticles in this study is justified by the fact that silica is widely used as filler in many types of composites.[19−25] Moreover, nano size fillers have an important specific surface and can potentially lead to a large number of attachment points with the polymer. Finally, monodisperse and spherical particles makes possible the use of mathematical models to describe subtle effects that can be of importance butare impossible to see with more "realistic" fillers, i.e. polydisperse and nonspherical systems. Thereafter, it should be possible to optimize the use of other more usual fillers and increase the properties of composites.

In the present study, small angle neutron scattering (SANS) and transmission electron microscopy (TEM) were used to characterize the local and mean particle distribution in the dry film. The SANS results are processed within the Percus−Yevick approximation.

Material and Methods

General Information. All experiments were conducted in distilled and deionized water. The chemical reagents were all analytical grade and used without further purification. The pH of solutions and suspensions was adjusted up to pH 9 with NaOH.

Synthesis and Characterization of Silica. Silica particles were grown from aqueous silicate solutions neutralized by nitric acid, as described by Iler.[26] Sodium silicate was produced by dissolving a pyrogenic silica into a concentrated NaOH solution to reach a molar ratio $x = SiO_2/Na_2O = 3.40$. The resulting silicate solution was thereafter diluted to a silica concentration of 0.57 M. The precipitation of silica was initiated by diluting an initial batch of silicate solution with water to a concentration of 0.004 M; this dilution lowered the pH to 9 and initiated the formation of silica nuclei. The synthesis was continued by adding simultaneously the 0.57 M silicate solution and a diluted nitric acid solution (0.27 M) at 90 °C still keeping the pH at 9. This procedure allows controll of the supersaturation and the resulting growth rate of the particles. Finally, the reaction mixture was allowed to ripen during slow cooling and storage for a few days at room temperature. The ripening stage allows reduction of the polydispersity index of the particles. According to the transmission electron micrograph (Figure 1), the particle hard-sphere diameter is $2R = 27$ nm. This value is consistent with the radius computed from the BET specific surface area (100 m^2/g). The hydrodynamic size and size distribution were determined at a volume fractionof 0.5% with dynamic light scattering (Malvern Zetasizer 4). The hydrodynamic diameter is $2R_H = 30$ nm and the polydispersity index is 1.07. The hydrodynamic size has also been measured by viscosimetry through the Einstein relation:

$$\eta/\eta_0 = 1 + 2.5\phi \quad (1)$$

where ϕ is the volume fraction of silica particles. The latter two methods lead exactly to the same value of the hydrodynamic size (30 nm).

Characterization of Polymer. The poly(vinyl alcohol) (PVA) used in this work was purchased from Fluka (cat. no. 9002-89-5). According to the supplier, this polymer has a molecular weight (MW) of 100 kg/mol and a degree of purity of 99% and hydrolysis of more than 99%. In the present study the polymer was used without further purification. Viscometry measurements have shown a MW of 107 kg/mol and a gyration radius $R_G = 15$ nm. The overlap concentration for this polymer is 8 g/L in water. The Flory parameter (χ) in semidilute condition was measured by osmometry. The experimental value was 0.499, which agrees well with $\chi = 0.494$ reported elsewhere.[27] In dilute condition, $\chi = 0.47$.[27] The mass of the elastic chains has been estimated from swelling experiments in water. This yields for the unfilled sample a MW of 7400 ± 400 g/mol. This value is similar to the value found by osmometry in the semidilute regime (6700 ± 400 g/mol).

Adsorption Isotherms. SiO_2 suspensions at initial pH 9 were mixed with PVA solutions (pH 9) of increasing concentrations. Five days were allowed for equilibrium at the end of which the final pH was measured. Next, the suspensions were centrifuged and the total organic carbon (TOC) of the supernatant was measured. Only experimental data with (initial TOC − equilibrium TOC)/initial TOC > 0.2 were taken as significant. The calibration curve was established with known concentrations of PVA. The standard deviation for three consecutive measurements was lower than 5%.

Film Formation. The films were prepared by mixing SiO_2 suspensions ($\phi = 0.02$, pH 9) with PVA solution (5% dwb, pH 9) in appropriate proportion to finish with solid mean volume fractions ($SiO_2/(SiO_2 + PVA)$) ranging from $\phi_{mean} = 0.03$ to 0.25 once all the solvent has been evaporated. The initial volume fractions, prior to any evaporation, ranged from 0.001 to 0.01. Dynamic light scattering (DLS) measurements show that the silica particles are still dispersed in the starting condition. Of course, the viscosity of the bulk polymer solution and the adsorbed polymer layer thickness have been taken into account when calculating the hydrodynamic radius of the particles by this method.

The evaporation was achieved at room temperature and free atmosphere and completed within 8 to 10 h. In the starting conditions, the molar chain/particle ratio is at least 200, and accordingly, the PVA surface coverage is well above saturation (see below).

Control experiments on the drying of silica without PVA have been conducted in a previous study reported in ref 28. They show perfectly dispersed particles on the whole range of ϕ_{mean} investigated in the present study.

Neutron Scattering. The neutron scattering experiments were performed at the ILL Institute (Grenoble, France) on the D11 instrument. The neutron wavelength was 6(±10) Å. Detector distance ranged from 5 to 36 m providing an experimental range of $0.002\ Å^{-1} < Q < 0.075\ Å^{-1}$, where Q is the scattering wave vector. The raw data were normalized and corrected for background with an unfilled PVA film.

Electron Microscopy. Transmission electron microscopy (TEM) sample preparation consisted of immobilizing the films

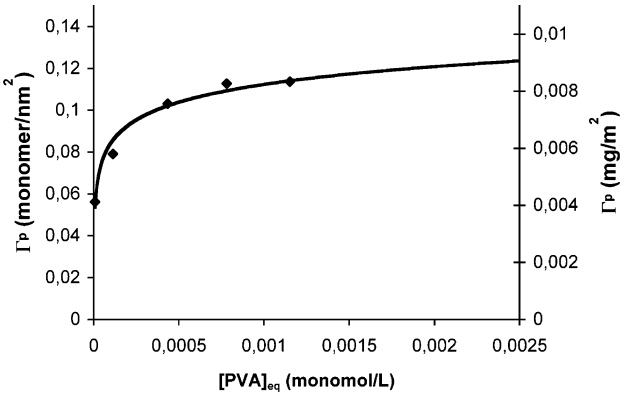

Figure 2. Adsorption isotherm of PVA 107 kg/mol on silica particles at pH 9.

in a resin and slicing the film with an ultramicrotome. The cross section was fixed onto a coated carbon grid. TEM examination was performed with a Philips instrument operating at 180 kV.

Results

Adsorption Isotherm. Earlier works on adsorption of neutral polymers on silica show that neutral polymers such as PEO adsorb on the hydrated silica surface through hydrogen bonds.[29,30] A similar behavior is expected with PVA but the better PVA−water interaction makes the surface less "attractive" to PVA. Since the surface density of silanol sites is low at pH 9,[31] low surface coverage is reported with PVA.[32,33] As shown in Figure 2, this is actually the case; the surface density at saturation is $\Gamma_p = 0.12$ monomer/nm^2 (0.008 mg/m^2). A weak (if any) steric protection against flocculation is expected.

Neutron Scattering. In the starting conditions, i.e., before any solvent evaporation, the chain/particle molar ratio is at least 200, well above the saturation density of 0.15 chain/particle found on absorption isotherms. The solvent was thereafter allowed to completely evaporate at room temperature. Finally, PVA matrixes filled with silica particles were recovered with mean solid volume fractions ($SiO_2/(SiO_2 + PVA)$) ranging from $\phi_{mean} = 0.03$ to 0.25 and thereafter analyzed by neutron scattering. (Note: To avoid any confusion, the volume fraction of the whole system will be herein referred to as the mean volume fraction (ϕ_{mean}) regardless of any local anisotropy while the volume fraction of the clusters will be referred to as the local volume fraction (ϕ_L).) The results are presented in Figure 3. The scattering patterns show two correlation peaks, indicative of a well-ordered arrangement of fairly monodisperse particles. According to Porod's law, smooth surfaces for spherical particles should lead to a −4 slope on a log−log scale. Although not obvious in Figure 3 because of the log scale, the experimental slope at high Q is −4, as expected from the particles shown in Figure 1. A −4 slope is also observed at low Q, indicating that large and dense clusters are present within the polymer matrix.

The experimental curves were modeled within the Percus−Yevick (PY) model where monodisperse hard-sphere particles are assumed to have a liquidlike distribution. In that case, the structure factor

$$S(Q)_p = 1 + 4\pi n \int_0^\infty [g(r) - 1] r^2 \frac{\sin(Qr)}{Qr}\, dr$$

yields an analytical solution (here, n is the number of particles per volume unit and g(r) is the radial distribution function) where the only variables are the volume fraction and the hard-sphere particle radius R. The later has been estimated from

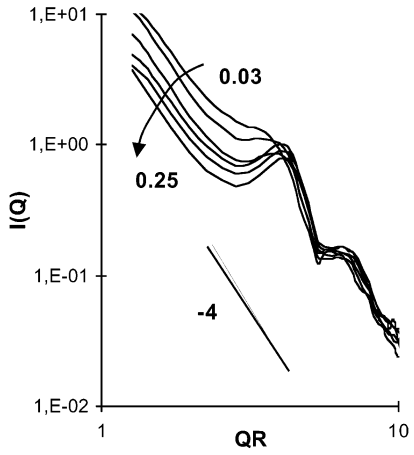

Figure 3. SANS of dry films with different ϕ_{mean} as indicated in the figure. The films were prepared by complete evaporation of the suspension's solvent. Initial suspension pH 9. The straight line indicates a −4 slope on a log−log scale.

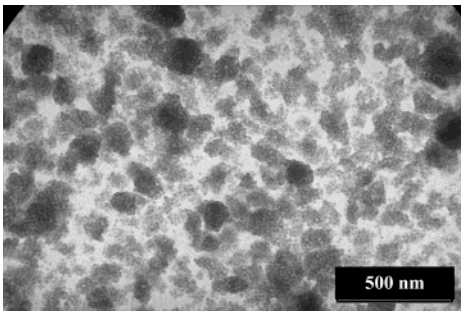

Figure 4. TEM micrograph of a cross section of the film sample with $\phi_{mean} = 0.03$.

Figure 1 to be $R = 13.5$ nm. On the other hand, the form factor for hard spheres is given by

$$P(Q)_p \approx \left[\frac{3j_1(QR)}{QR}\right]^2$$

where $j_i(QR)$ is the first-order Bessel function $j_1(QR) = (\sin(QR) - QR\cos(QR))/(QR)^2$. The total scattered intensity is $I(Q) \approx P(Q)S(Q)$.

Transmission electron microscopy (TEM) was performed on the composites with different ϕ_{mean}. For practical reasons, only one TEM micrograph is reported in this study ($\phi_{mean} = 0.03$). The micrograph in Figure 4 shows quite spherical clusters. Clearly, the primary particles are not homogeneously distributed within the polymer matrix and rather tend to "clusterize" into clusters made up of a large number of well-ordered primary particles. Accordingly, the scattering curves must be modeled by considering two length scales: the first one for the primary particles within the clusters and the second one for the clusters within the polymer material. The global scattered intensity is then given by[7]

$$I(Q)/N = P(Q)_p[(N-1)P(Q)_c + S(Q)_p]$$

where N is the number of particles/cluster, and $P(Q)_c$ is the form factor for the clusters having a radius R_c. As a refinement, the size polydispersity of clusters (see Figure 4) can also be taken into account within the form factor as described elsewhere.[34] Then, the complete modeling of the experimental scattering curves can be achieved, as long as one knows the hard-sphere radius of clusters (R_c) and primary particles (R), and with the volume fraction of the primary particles in the clusters (i.e. the

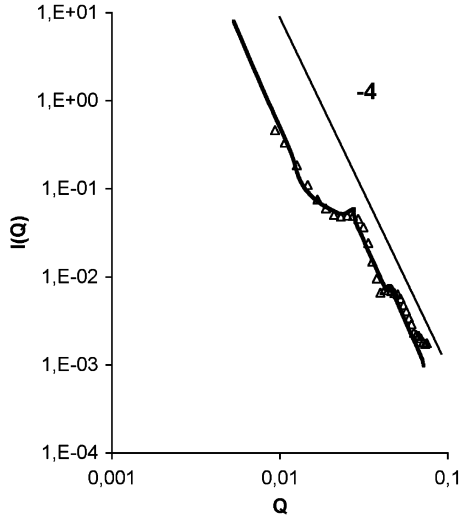

Figure 5. Fit results of SANS data (symbols) for the film with $\phi_{mean} = 0.05$, using the PY model (solid line) taking $R = 13.5$ nm and $R_c = 110 \pm 10$ (see text for details). The volume fraction in the clusters is taken as an adjustable parameter. The concordance between the correlation peaks (PY vs experimental) is possible only when the local volume fraction in clusters is set to $\phi_l = 0.50$.

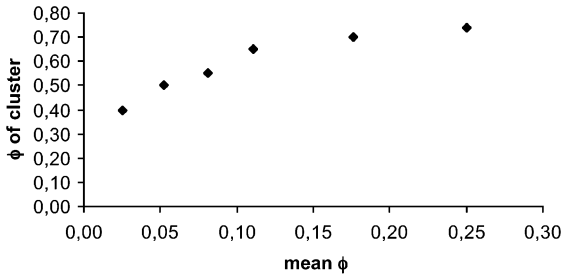

Figure 6. Fit of the local volume fraction in the clusters (ϕ_L) against the mean volume fraction in films (ϕ_{mean}). ϕ_L has been deduced from the volume fraction needed to be input in the PY model to achieve perfect fit between the PY and experimental correlation peaks.

local volume fraction) being taken as an adjustable parameter. One example of such modeling is presented in Figure 5. For this particular sample, the mean cluster radius $R_c = 110 \pm 10$ nm (according to TEM micrographs not shown), the volume fraction of the clusters $\phi_{mean} = 0.05$, and again $R = 13.5$ nm. In the present case, the modeled curve best fits the experimental correlation peaks when $\phi_L = 0.50$. This is one decade over ϕ_{mean}.

Similar data processing at other ϕ_{mean} values shows in Figure 6 that the volume fraction of clusters increases with ϕ_{mean} up to 0.74, indicating an hexagonal compact arrangement (maximum packing fraction). Assuming spherical and monodisperse primary particles, the surface-to-surface distance (H) of particles within clusters can be computed from the position of the Bragg peaks for a hexagonal compact arrangement:

$$H = [(3/2)^{1/2}2\pi/Q] - 2R \qquad (2)$$

The surface-to-surface distance against ϕ_{mean} is presented in Figure 7. The results in both Figures clearly show a densification process of clusters as ϕ_{mean} increases. The clusters have already reached the maximum packing arrangement at $\phi_{mean} = 0.25$.

Moreover, the size of the clusters can also be calculated from the scattering curves. According to Porod's law the surface area (s) of a smooth scattering object can be calculated from the region where the slope is -4 on a log$-$log scale. Porod's law is usually used only at high Q (lim $Q \rightarrow \infty$) but actually remains valid at every Q domain where $I(Q)$ goes like Q^{-4} since the

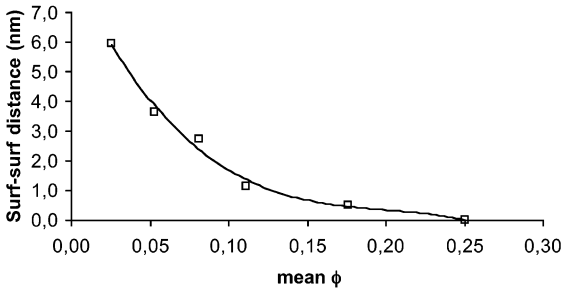

Figure 7. Particle surface-to-surface distance within clusters computed with eq 2 by taking the maximum Q of correlation peak values from SANS data in Figure 3.

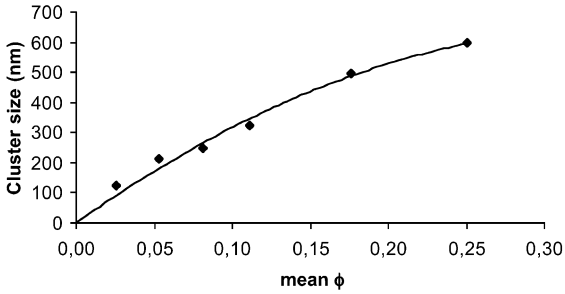

Figure 8. Cluster size computed with eq 3 against the mean volume fraction.

definition of high or low Q is somewhat arbitrary. The ratio between the surface area of clusters (-4 slope at low Q) and that of primary particles (-4 slope at high Q) is given by

$$\frac{s_c}{s_p} = \frac{[I(Q)Q^4]_c \rho_p V_c}{[I(Q)Q^4]_p \rho_c V_p}$$

where V_p and ρ_p are the volume and the density of the primary particles, respectively, and where V_c and ρ_c are related to the clusters. Since the ratio s_c/V_c is proportional to the cluster diameter d_c

$$\frac{d_c}{2R} = \frac{[I(Q)Q^4]_p \rho_c}{[I(Q)Q^4]_c \rho_p} \qquad (3)$$

The cluster sizes d_c at different ϕ_{mean} values were then determined from the neutron curves where the Q^{-4} behavior is observed. As shown in Figure 8, the clusters reach a large size, more than one decade over that of primary particles, even at very low ϕ_{mean}. The cluster size seems to level off at 600 nm. The standard error in the data in this figure is estimated to be about $\pm 20\%$.

The cluster size, as estimated from transmission electron microscopy (Figure 4 and others not shown), is in close agreement with the size found from neutron scattering.

To better understand the effect of the drying kinetics on the cluster formation as solvent evaporation continues, neutron scattering measurements were conducted at different times and different ϕ'_{mean} values, where ϕ'_{mean} is the mean silica volume fraction in the suspension when not all the solvent has been evaporated (SiO_2/(SiO_2 + PVA + water)). For these experiments, if all the solvent had been allowed to evaporate, the final ϕ_{mean} would have been 0.25. The ϕ'_{mean} values were previously adjusted at 0.03, 0.09, and 0.15 by allowing some of the solvent to evaporate and by stopping the evaporation once the target volume fractions were reached. The suspensions (SiO_2 + PVA + water) were maintained in these conditions for 8 h, and

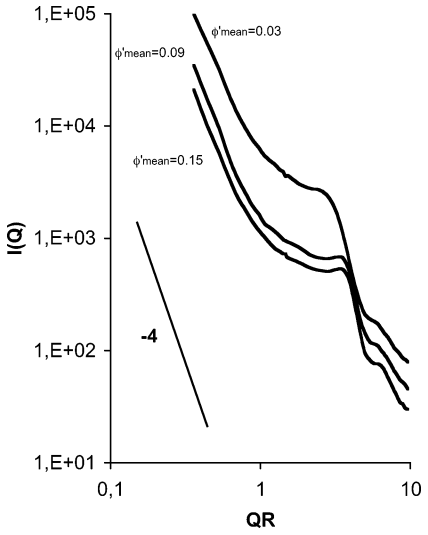

Figure 9. SANS of SiO_2 + PVA suspensions before complete evaporation of the solvent ($\phi'_{mean} = 0.03, 0.09, 0.15$). The suspensions where left at rest for 8 h before the measurements were taken. Should all the solvent be allowed to evaporate the final mean volume fraction would be 0.25.

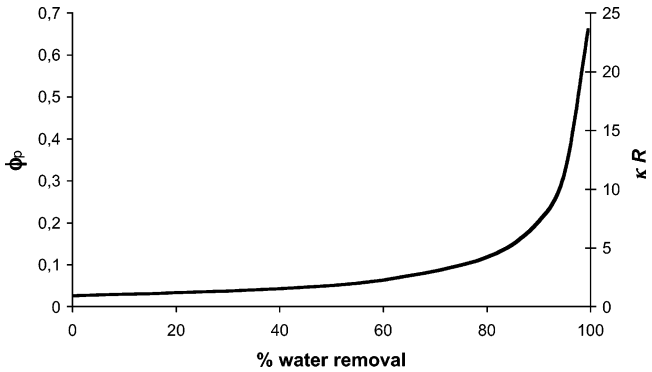

Figure 10. Evolution of the polymer concentration and salt content as evaporation progresses for the suspension corresponding to $\phi_{mean} = 0.25$.

thereafter monitored by SANS. The results are reported in Figures 9 and 10. The particles used here were somewhat larger than those used previously ($R = 17$ nm instead of 13.5 nm). This is why the Bragg peaks in Figures 9 and 10 do not match those shown in earlier figures.

The results presented in Figure 9 show that the primary particles collapse into individual clusters before all the solvent has been evaporated. Indeed, according to the SANS measurements, the clusters appear at a very low volume fraction ($\phi'_{mean} \leq 0.031$). Accordingly, the "clusterization" takes place very early in the drying process. As shown by the displacement of the main correlation peak, further evaporation, although incomplete, makes the clusters denser, i.e., the volume fraction of clusters increases with the extent of evaporation.

Discussion

As reported above, the nanosize silica particles can self-assemble into a well-ordered arrangement while the suspension concentrates and a dry composite film is formed with clusters of particles, rather than well-dispersed primary particles, embedded in the polymer matrix. It also has been shown that the final overall structure depends on how fast the evaporation process takes place. This behavior is certainly of importance in regard to the properties of composite materials or self-assembled systems and is debated below.

The self-assembly process observed here leads to clusters with well-defined size and intracluster surface-to-surface distances which both can be adjusted by controlling the mean volume fraction of the composite. The transition from dispersed particles to dense clusters is well-documented in the literature for dilute polymer−particle suspensions in similar experimental conditions and is known to be ionic strength dependent.[9] However, in such dilute systems no evidence of cluster "densification" and microphase separation has been reported so far. Of course in the present study, this rearrangement can only take place before complete evaporation of the solvent and occurs at very low mean volume fractions, according to Figures 4, 5, and 9. The behavior observed here shows some interesting similarities with the phase behavior observed on the evaporative drying of droplets of hard-sphere colloidal polymeric particles and nonadsorbing polymer, as reported very recently.[35] Our initial conditions are comparable to the "fluid sample case" described in ref 35 and lead to a sol of colloidal aggregates upon drying, as described in this reference and observed in the present study. In ref 35 the depletion attraction is presumed to induce a phase transition as drying progresses. This point is further debated here.

The driving potential energy for clustering (or aggregation) is the sum of the attractive depletion and van der Waals potentials. The long-range electrostatic and short-range steric potentials oppose the two former potentials. Prior to evaporation, the primary particles are dispersed. Accordingly, the repulsive energies are larger than the attractive ones. At the end of the evaporation process, clusters are observed. Clearly, at some point upon drying the attraction overcomes the repulsion, and the particles collapse, leading to a microphase separation. In the following, we show how decreasing electrostatic energy and increasing attractive energy upon drying can lead to the formation of clusters, and how involved the PVA/SiO_2 interaction is.

The nonretarded van der Waals energy interaction curve between spherical particles can be modeled through[2]

$$\frac{V_{(r)}^{vdW}}{kT} = -\frac{A}{6kT}\left[\frac{2R^2}{r^2-4R^2} + \frac{2R^2}{r^2} + \ln\left(\frac{r^2-4R^2}{r^2}\right)\right] \quad (4)$$

where r is the center-to-center distance between two particles, kT is the thermal energy, and A is the Hamaker constant. The Hamaker constant has been computed according to the method described elsewhere[36,37] to account for the increasing polymer concentration in the bulk as evaporation progresses.

The electrostatic energy between particles in a 1:1 electrolyte can be expressed as[38]

$$\frac{V_{(r)}^{el}}{kT} = \frac{(Z_{eff})^2 L_B}{r}\frac{\exp[-\kappa(r-2R)]}{(1+\kappa R)^2} \qquad (\kappa R < 10,\ r/R > 1) \quad (5)$$

where Z_{eff} is the effective charge of the particle as defined by the charge renormalization theory,[37] L_B is the Bjerrum length (0.7 nm in water at 25 °C), and κ^{-1} is the Debye length (κ^{-1} (nm) $= 0.3045/I^{0.5}$ in water at 25 °C). As reported elsewhere for silica[28] and according to theoretical models on ionic condensation,[38] the effective charge of silica can be calculated by $Z_{eff} = 4R/L_B$ and is nearly constant for κR values between 0.1 and 3. As shown in Figure 10, κR in eq 5 depends on the extent of the evaporation process and remains below 3−4 until high percentages of water removal are reached (>70%).

The depletion effects in a semidilute polymer solution can be described from the Asukara−Oosawa model. For spherical

particles, the effective interaction is given by[39]

$$\frac{V_{(r)}^{\text{dep}}}{kT} = -\frac{\Pi_p}{kT}\frac{\pi}{4}\left[2R\lambda(r-2R\lambda)^2 + \frac{1}{3}(r-2R\lambda)^3\right] \quad (2R \le r \le 2(R+R_p),\ R >> R_p) \quad (6)$$

where Π_p is the polymer osmotic pressure, $\lambda = 1 + R_p/R$, and R_p is the effective hard-sphere radius that describes the polymer.

In the semidilute regime, overlapping polymer coils lead to a new size scale determined by the correlation length ξ.[40] The polymer can be viewed as a close-packed system of noninteracting spheres (blobs) of size ξ, whose steric avoidance of embedded particles gives rise to the depletion effect. Then we identify R_p with $\pi\xi/2$, which yields $\lambda = 1 + \pi\xi/(2R)$. The correlation length is related to the density of segments in the bulk as[40]

$$\xi = \frac{b}{(12\upsilon\rho_p N)^{1/2}} \quad (7)$$

where υ is the excluded volume parameter, ρ_p is the number density of polymer, N is the number of segments per polymer chain, and b is the effective bond length fixed at 0.25 nm based on molecular models. The excluded volume parameter in eq 7 can be approximated by[40] $\upsilon \cong (1 - 2\chi)b^3$. With use of scaling arguments, the osmotic pressure in the semidilute regime can be modeled by taking the bulk as an ideal gas of spherical blobs with diameter $\pi\xi$.[39] Accordingly, Π_p scales as $1/\xi^3$, as described in ref 40.

More recent analytical and numerical equations can also be used to calculate the depletion energy. These equations, fully described in ref 1, are more sophisticated than eq 6 since they can take into account the compressibility of the adsorbed polymer layer as well as the interpenetration domain between the adsorbed and bulk polymer. Nevertheless, for the sake of simplicity, we decided to use eq 6 instead since all the equations we tried led to very similar results, no matter their degree of sophistication. This is mainly due to the very low surface density and polymer concentration in the adsorbed layer in the present experimental conditions. For the same reason, steric interactions are not taken into account in this modeling. According to equations reported in ref 3, this energy is lower than a few tens of kT within the interpenetration domain (surface-to-surface distance down to 3−5 nm), so they are neglected here, although it can lead to steep repulsion at smaller distances when the surface coverage is high.

Assuming the superposition approximation to be valid, the potential energy diagram can be expressed as the sum of eqs 4−6. In Figure 11 are reported the energy diagrams at different stages of the drying process (different ϕ'_{mean}) for the suspension corresponding to a final mean volume fraction of 0.25. This modeling shows that a phase transition is theoretically expected for ϕ'_{mean} near 0.023 (corresponding to 60% of water removal). The experimental data in Figure 9 consistently show that clusters are already present at $\phi'_{\text{mean}} = 0.030$. From the modeling above, it clearly appears that the transition from a repulsive to an attractive potential comes from the simultaneous increase of depletion (through the increase of polymer volume fraction) and the decrease of the electrostatic contribution (through the increase of κR) as evaporation progresses (see Figure 10). Our model shows that even a pronounced reduction of the dielectric constant of the bulk medium (down to 20, instead of 78) has no noticeable effect on the volume fraction at which the phase transition occurs; it reduces the magnitude of both $V_{(r)}^{\text{vdW}}$ and $V_{(r)}^{\text{el}}$ in such a way that the phase transition is predicted at the same critical volume fraction.

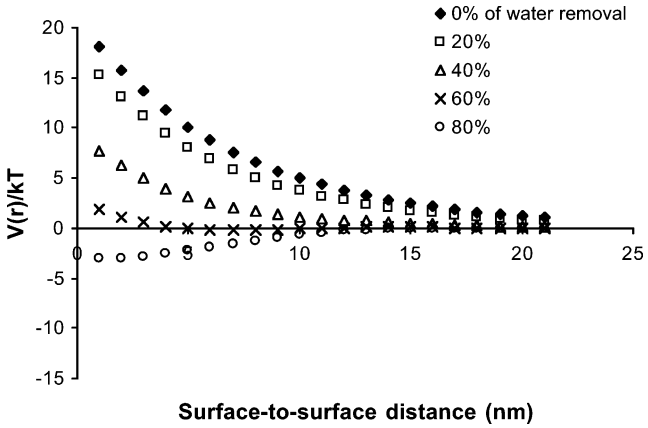

Figure 11. Energy diagrams at different percentages of water removal. At 0% of water removal, $\phi'_{\text{mean}} = 0.01$; at 20%, $\phi'_{\text{mean}} = 0.012$; at 40%, $\phi'_{\text{mean}} = 0.015$; at 60%, $\phi'_{\text{mean}} = 0.022$, at 80%, $\phi'_{\text{mean}} = 0.044$; at 100%, $\phi'_{\text{mean}} = \phi_{\text{mean}} = 0.25$. $V_{(r)} = V_{(r)}^{\text{vdW}} + V_{(r)}^{\text{el}} + V_{(r)}^{\text{dep}}$.

As reported in Figure 10, the ionic strength of the PVA−SiO_2 suspension (proportional to κR) increases upon evaporation. The ionic strength in the present case comes from the bulk solution of the mother SiO_2 suspension and from the effective charge (Z_{eff}) of the SiO_2 particles. Accordingly, the higher the silica contents in the initial SiO_2−PVA suspension (before evaporation), the higher the ionic strength in the suspension, at a given evaporation stage. The increasing ionic strength is known to influence the surface chemistry of silica through the following surface equilibriums:

$$\equiv\text{Si}-\text{OH} \leftrightarrow \equiv\text{Si}-\text{O}^- + \text{H}^+ \quad (8)$$

$$\equiv\text{Si}-\text{ONa} \leftrightarrow \equiv\text{Si}-\text{O}^- + \text{Na}^+ \quad (9)$$

As evaporation progresses, the ionic strength increases up to 0.05−0.3 M (depending on the ϕ_{mean} to be reached) and eq 9 is shifted to the left while eq 8 is shifted to the right, as a result of which the surface density of silanol sites is reduced. Since nonionic polymers adsorb on silica through H-bounding involving silanols surface groups, a lower Γ_p is expected as the ionic strength increases. Such behavior is well referenced in the literature.[41] It is known that reducing Γ_p reduces the layer thickness.[42] A higher ionic strength can also decrease the adsorbed layer thickness, further reducing the protection against aggregation.[41,43] These two effects (lowering of polymer surface density and layer thickness) could explain the decreasing surface-to-surface distance as ϕ_{mean} increases (see Figure 7). Such combined effects cannot be easily taken into account by analytical equations to simultaneously model both the aggregation *and* the cluster densification as evaporation progresses.

Conclusion

The structure of SiO_2/PVA composites investigated in this study depends mainly on the ionic strength. As evaporation progresses, the ionic strength increases. This increase has two effects. First, the relative magnitude of the repulsive electrostatic forces is gradually reduced upon solvent evaporation. The depletion forces are expected to be the driving force of the clustering as repulsion vanishes. Second, the increase of ionic strength reduces the surface affinity of silica for the polymer, which effect reduces the protective short-range (steric) repulsion as the polymer desorbs. Both effects are responsible for the

occurrence of microphase separation into well-ordered clusters (first effect) and for the well-defined surface-to-surface distance within the clusters (second effect). Of course, the higher the mean volume fraction in the dry film, the more important these effects are. In other words, the higher the mean volume fraction, the larger the size of the clusters and the lower the surface-to-surface distance within the clusters.

Acknowledgment. The authors would like to acknowledge Peter Lindner and Joanes Zipfel (Institut Laue-Langevin, Grenoble) for technical support on the D11 instrument and Agnès Lejeune for supplying TEM micrographs. The Ministère des Relations Internationales du Québec, NanoQuébec, as well as NSERC-International Opportunity Fund are also acknowledged for financial support through research grants. This work was done with the neutron beam of the Institut Laue-Langevin.

References and Notes

(1) Fleer, G. J.; Cohen Stuart, M. A.; Scheutjens, J. M.; Cosgrove, T.; Vincent *Polymer at Interfaces*; Chapman & Hall: London, 1993.

(2) Russel, W. B.; Saville, D. A.; Schowalter, W. R. In *Colloidal Dispersions*; Cambridge University Press: Cambridge UK, 1989; Chapters 4−5.

(3) Hunter R. In *Fundations of colloid science*; Clarendon Press: Oxford, UK, 1995, Vol. 1, Chapters 6−7.

(4) Wind, B.; Killman, E. *Colloid Polym. Sci.* **1998**, *276*, 912.

(5) Lafuma, F.; Wong, K.; Cabane, B. *J. Colloid Interface Sci.* **1991**, *143*, 9.

(6) Wong, K.; Cabane, B.; Somasundaran, P. *Colloids Surf.* **1988**, *30*, 355.

(7) Cabane, B.; Wong, K.; Wang, T. K.; Lafuma, F. *Colloid Polym. Sci.* **1988**, *266*, 101.

(8) Wong, K.; Cabane, B.; Duplessix, R. *J. Colloid Interface Sci.* **1988**, *123*, 466.

(9) Wong, K.; Lixon, P.; Lafuma, F.; Lindner, P.; Aguerre Charriol, O.; Cabane, B. *J. Colloid Interface Sci.* **1992**, *153*, 55.

(10) Rudhardt, D.; Bechinger, C.; Leiderer, P. *J. Phys.*: *Condens. Matter* **1999**, *11*, 10073.

(11) Biggs, S.; Burns, J. L.; Yan, Y.; Jameson, G. J.; Jenkings, P. *Langmuir* **2000**, *16*, 9242.

(12) Burns, J. L.; Yan, Y.; Jameson, G. J.; Biggs, S. *J. Colloid Interface Sci.* **2002**, *247*, 24.

(13) Milling, A. J.; Kendall, K. *Langmuir* **2000**, *16*, 5106.

(14) Guth, E.; Gold, O. *Phys. Rev.* **1938**, *53*, 322.

(15) Osman, M. A.; Atallah, A.; Müller, M.; Suter U. W. *Polymer* **2001**, *42*, 6545.

(16) Lu, Y.; Yang, Y.; Sellinger, A.; Lu, M.; Huang, J.; Fan, H.; Haddad, R.; Lopez, G.; Burns, A.; Sasaki, D.; Shelnutt, J.; Brinker C. J. *Nature* **2001**, *410*, 913.

(17) Jang, J.; Park, H. *J. Appl. Polym. Sci.* **2002**, *83*, 1817.

(18) Becker, C.; Kutsch, B.; Krug, H.; Kaddami, H. *J. Sol−Gel Sci. Technol.* **1998**, *13*, 499.

(19) Hajji, P.; David, L.; Gerard, J. F.; Pascault, J. P.; Vigier, G. *J. Polym. Sci.* **1999**, *37*, 3172.

(20) Xu, X.; Littrel, K.; Ji, S.; Pickles, D. G.; Risen, W. M. *J. Non-Cryst. Solids* **2001**, *288* 184.

(21) McCarthy, D. W.; Mark, J. E.; Schaeffer, D. W. *J. Polym. Sci.* **1998**, *36*, 1167.

(22) Bokobza, L.,*Macromol. Symp.* **2001**, *171*, 163.

(23) Deng, Q.; Hahn, J. R.; Stasser, J.; Preston, J. D.; Burns, G. T. *Rubber Chem. Technol.* **2000**, *73*, 647.

(24) Nunes, R. C. R.; Fonseca, J. L. C.; Pereira, M. R. *Polym. Test.* **2000**, *19*, 93.

(25) Botti, A.; Pyckhout-Hintzen, W.; Richter, D.; Straube, E. *Physica A* **2002**, *304*, 230.

(26) Iler, R. K. *The chemistry of Silica*; Wiley: New York, 1979.

(27) Lewandowska K.; Staszewska D. U.; Bohdanecky M. *Eur. Polym. J.* **2001**, *37*, 25.

(28) Persello, J. Surface and Interface Structure of Silicas. In *Adsorption on Silica Surfaces*; Papirer, E., Ed.; Marcel Dekker: New York, 2000.

(29) Van der Beek, G. P.; Cohen-Stuart, M. A. *J. Phys. (France)* **1988**, *49*, 1449.

(30) Cohen-Stuart, M. A.; Fleer, G. J.; Scheutjen, J. M. H. M. *J. Colloid Interface Sci.* **1989**, *97*, 526.

(31) Foissy A.; Persello J. *The surface properties of Silicas*; Legrand, A. P., Ed.; John Wiley and Sons Ltd.: New York, 1998; pp 365−414.

(32) Eremenko, B. V.; Malysheva, O. D. R.; Kutsevol, N. V.; Zeltonozskaya, T. B. *Colloids Surf.* **1995**, *98*, 19.

(33) Santhiya, D.; Subramanian, S.; Natarajan, K. A.; Malghan, S. G. *J. Colloid Interface Sci.* **1999**, *216*, 143.

(34) Guinier A. *Théorie et technique de la radiocristallographie*, 3rd ed.; Dunod: Paris, France, 1964.

(35) Haw, M. D.; Gillie, M.; Poon, W. C. K. *Langmuir* **2002**, *18*, 1626.

(36) Israelachvili, J. *Intermolecular and surfaces forces*, 2nd ed.; Academic Press: London, UK, 1991; Chapter 11.

(37) Israelachvili, J. *Proc. Phys. Soc. London* **1972**, *39*, A331.

(38) Belloni, L. *Colloids Surf. A* **1998**, *140*, 227

(39) Verma, R.; Crocker, J. C.; Lubensky, T. C.; Yodh, A. C. *Macromolecules* **2000**, *33*, 177.

(40) De Gennes, P. G. *Scalling Concepts in Polymer Physics*; Cornell University Press: Ithaca, NY, 1979.

(41) Zaman, A. A. *Colloid Polym. Sci.* **2000**, *278*, 1187.

(42) Wind, B.; Killmann, E. *Colloid Polym. Sci.* **1998**, *276*, 903.

(43) Pattanayek, S. K.; Juvekar, V. A. *Macromolecules* **2002**, *35*, 9574.